



HAL
open science

Investigation of structural and ionic conductivity in the new organic-inorganic bromide: $[(C_3H_7)_4P]_2Cd_2Br_6$

H. Elgahami, M. Ajili, Thierry Roisnel, A. Oueslati

► To cite this version:

H. Elgahami, M. Ajili, Thierry Roisnel, A. Oueslati. Investigation of structural and ionic conductivity in the new organic-inorganic bromide: $[(C_3H_7)_4P]_2Cd_2Br_6$. *Journal of Solid State Chemistry*, 2022, 311, pp.123108. 10.1016/j.jssc.2022.123108 . hal-03661091

HAL Id: hal-03661091

<https://hal.science/hal-03661091>

Submitted on 11 May 2022

HAL is a multi-disciplinary open access archive for the deposit and dissemination of scientific research documents, whether they are published or not. The documents may come from teaching and research institutions in France or abroad, or from public or private research centers.

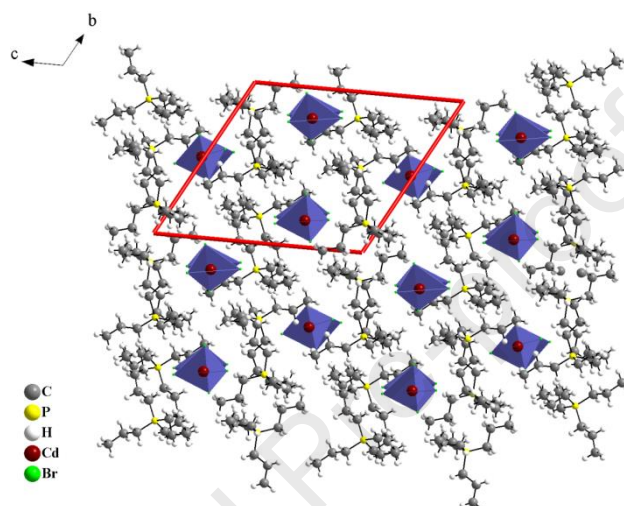
L'archive ouverte pluridisciplinaire **HAL**, est destinée au dépôt et à la diffusion de documents scientifiques de niveau recherche, publiés ou non, émanant des établissements d'enseignement et de recherche français ou étrangers, des laboratoires publics ou privés.



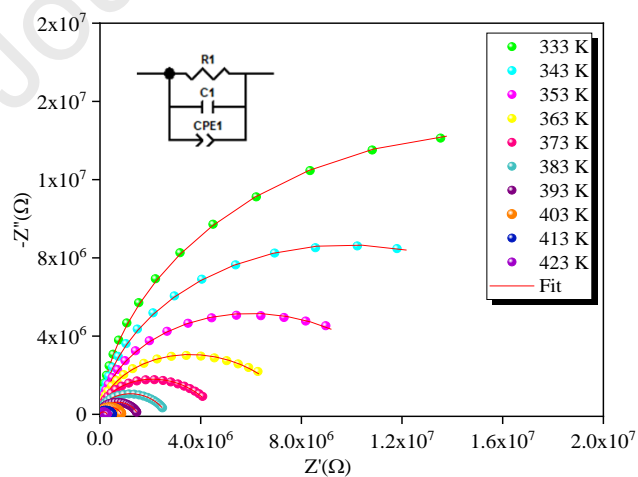
Distributed under a Creative Commons Attribution - NonCommercial 4.0 International License

Investigation of structural and ionic conductivity in the new organic-inorganic bromide: $[(C_3H_7)_4P]_2Cd_2Br_6$

H. Elgahami^{*1}, M. Ajili¹, T. Roisnel², A. Oueslati¹



Projection along the a axis of the atomic arrangement of $[(C_3H_7)_4P]_2Cd_2Br_6$



Observed and calculated impedance complex plane plots of the $[(C_3H_7)_4P]_2Cd_2Br_6$ compound

Authors' contributions

Hanen Elgahami: Writing- Original draft preparation

Mouna Ajili: Writing- Original draft preparation,

Thierry Roisnel: Investigation, Software, Visualization,

Abderrazek Oueslati: Visualization, Validation, Reviewing and Editing

Journal Pre-proof

Investigation of structural and ionic conductivity in the new organic-inorganic bromide: $[(C_3H_7)_4P]_2Cd_2Br_6$

H. Elgahami^{*1}, M. Ajili¹, T. Roisnel², A. Oueslati¹

¹Laboratory for Spectroscopic Characterization and Optics of Materials, Faculty of Sciences, University of Sfax, B. P. 1171, 3000 Sfax, Tunisia

²ISCR (Institut des Sciences Chimiques de Rennes)

* Corresponding author.

E-mail address: hanengahami1993@gmail.com

Abstract

The organic-inorganic compounds with alkylphosphonium groups were employed in many fields of applications as reported in various studies. Furthermore, these materials had shown diverse transitions depending on the preparation process. In this paper, a novel organic-inorganic hybrid $[(C_3H_7)_4P]_2Cd_2Br_6$, has been synthesized and characterized by single crystal X-ray diffraction, differential scanning calorimetry and complex impedance spectroscopy measurement. The crystal structure refinement shows that the crystallization of the $[(C_3H_7)_4P]_2Cd_2Br_6$ compound was achieved in the Triclinic system (P-1: space group, Ci: Schoenflies's nomenclature) with the following unit cell dimensions: $a = 13.662(3) \text{ \AA}$, $b = 16.146(4) \text{ \AA}$, $c = 16.857(4) \text{ \AA}$, $\alpha = 114.867(6)^\circ$, $\beta = 91.650(8)^\circ$, $\gamma = 114.357(7)^\circ$ and $Z = 3$. The differential scanning calorimetry (DSC) analysis shows an endothermic peak at 364 K upon heating which attributed to a structural phase transition. The study of the AC conductivity and the dielectric properties confirm the existence of the phase transition. Complex impedance spectroscopic analysis indicated both, the presence of bulk contribution and non-Debye type in the material. The bulk resistance decreases with increasing temperature indicating a typical semiconductor behavior. The thermal evolution of the conductivity is found to obey the Arrhenius law with activation energies, 0.55 eV in region I and 0.78 eV in region II.

Keywords: $[(C_3H_7)_4P]_2Cd_2Br_6$, Organic-inorganic, Crystal structure, DSC, Electrical properties.

I. Introduction

Owing to their technological aspects and potential applications in various areas such as optical, ferroelectric, magnetic, optoelectronics. Organic–inorganic hybrid materials have taken more attention in the last decade by researchers [1-3]. In fact, in the last few years, significant efforts have been dedicated to the synthesis of new organic-inorganic compounds with tetraalkylphosphonium groups [4-6]. These materials have already revealed multiple phase transitions generally associated to the reorientational dynamics of the substitute phosphonium group. Moreover, recent electric and dielectric studies of these crystals have shown that the majority of these phase transitions were responsible for multiple anomalies in the conductivity and dielectric behaviors that are both very sensitive to the temperature as well as to the external electric field [7-9].

In this aim, the interest in our laboratory is focused on the investigation of chemical and physical properties of hybrid materials with the organic tetraalkylphosphonium cation of the general formula $[(C_nH_{2n+1})_4P]^+$. The most interested properties, were proven in cations with $n=1$ $[(CH_3)_4P]^+$, $n=2$ $[(C_2H_5)_4P]^+$, $n=3$ $[(C_3H_7)_4P]^+$, and $n=4$ $[(C_4H_9)_4P]^+$ [10-13]. In the present paper, we are interested to prepare a new organic-inorganic compound $[(C_3H_7)_4P]_2Cd_2Br_6$, describe their crystal structure using the X-ray diffraction single crystal method, to study the phase transitions by the differential scanning calorimetry (DSC) and to evaluate the polar properties of the bis tetrapropylphosphonium hexabromo-dicadmate hybrid through electric and dielectric response.

II. Experimental

All starting materials were commercially available reagents of analytical grade from Sigma Aldrich and used without further purification.

The bis-tetrapropylphosphonium hexabromo-dicadmate $[(C_3H_7)_4P]_2Cd_2Br_6$ crystals were grown by slow evaporation at room temperature. The solution of the title compound was obtained by mixing a stoichiometric molar ratio of $[(C_3H_7)_4P]Br$ (Purity 95%; FLUKA) and $CdBr_2$ (Purity 98%; FLUKA) in aqueous solution in molar ratio 2:1 according to the following equation:



The obtained solution was evaporated at room temperature and after several days colourless prism monocrystals were obtained.

A suitable crystal for X-ray diffraction, single crystal experiment was selected and mounted with a cryoloop on the goniometer head of a APEX II Kappa-CCD (Bruker-AXS) diffractometer equipped with a CCD plate detector, using Mo-K α radiation ($\lambda = 0.71073 \text{ \AA}$, graphite monochromator) at $T = 150 (2) \text{ K}$. Crystal structure has been described in triclinic symmetry and centric space group $P-1(C_i)$. Cell parameters have been refined as follows: $a = 13.662 (3) \text{ \AA}$, $b = 16.146 (4) \text{ \AA}$, $c = 16.857 (4) \text{ \AA}$, $\alpha = 114.867 (6)^\circ$, $\beta = 91.650 (8)^\circ$, $\gamma = 114.357 (7)^\circ$, $V = 2980.1 (12) \text{ \AA}^3$. Number of formula unit Z is equal to 3 and calculated density d and absorption coefficient μ values are 1.857 g.cm^{-3} and 7.197 mm^{-1} respectively. Crystal structure was solved by dual-space algorithm using SHELXT program [14], and then refined with full-matrix least-squares methods based on F^2 (SHELXL program [15]). All non-Hydrogen atoms were refined with anisotropic atomic displacement parameters. H atoms

were finally included in their calculated positions and treated as riding on their parent atom with constrained thermal parameters. A final refinement on F^2 with 3573 unique intensities and 264 parameters converged at $\omega R(F^2) = 0.242$ ($R_F = 0.087$) for 2997 observed reflections with ($I > 2\sigma$). The details of the key crystallographic information, the fractional atomic coordinates and equivalent isotropic displacement parameters (\AA^2) were summarized in Tables 1 and 2 respectively.

Atomic coordinates anisotropic displacement parameters, tables for all bond distances, and angles have been deposited at the Cambridge Crystallographic Data Centre (deposition number: CCDC 2141595). Copies of the data can be obtained, free of charge, on application to the Director, CCDC, 12 Union Road, Cambridge CB2 1EZ, UK (Fax: (44) 1223 336-408; email: deposit@ccdc.cam.ac.uk).

The Differential Scanning Calorimetry (DSC) measurement was carried out using a Perkin Elmer DSC 4000 calorimeter, by putting the powder sample (about 6.100 mg for a scanning rate of 5.00 °C/min) in an aluminum capsule. The DSC was studied in the temperature range from 300 to 440 K under inert atmosphere (nitrogen gas).

In order to perform the electrical measurements, a pressed pellet of 8 mm diameter and 1.1 mm thickness of the powdered sample was prepared using a hydraulic press at a pressure of 5000 kg cm⁻². The measurements of the electric impedance were registered in the frequency ranging from 100 Hz to 5 MHz and in the temperature range 333-423 K using 1260 Solartron Impedance Analyzer.

III. Results and discussion

1. Crystal structure description

Figure 1 shows that the asymmetric unit $[(C_3H_7)_4P]_2Cd_2Br_6$ consists one and half of $[Cd_2Br_6]^{2-}$ un-equivalent dimers and three $[(C_3H_7)_4P]^+$ cations.

The structural arrangement of the title compound can be described by an alternation of organic and inorganic layers along the [100] direction, made up of $[(C_3H_7)_4P]^+$ and $[Cd_2Br_6]^{2-}$ atom groups, as shown in Fig. 2. The details of the principal inter-atomic distances and angles for anionic and cationic groups are summarized in table 3.

The cohesion in the crystal is ensured by Van Der Waals and electrostatic interactions, between the bromure atoms of the anionic groups and the phosphorus atoms of the cationic groups.

The Cd–Br bond lengths vary from 2.504 (6) to 2.678 (6) Å with a mean value of 2.595 Å. The Br–Cd–Br angle values are in the range of 90.6 (2) ° - 122.4 (2) ° with the mean value of 108.92°. The $[(C_3H_7)_4P]^+$ cation is described by a broken cross configuration. The P–C bond lengths vary from 1.70 (5) to 1.81 (4) Å, while the C–C bond lengths are in the range of 1.46 (5) - 1.57(6) Å. The C–P–C angles are in the range of 107 (2) - 111 (2) °. The C–C–P angles are in the range of 115 (2) ° - 122 (3) °. As for the C–C–C angles, they vary from 109 (3) ° to 120 (4) °.

2. Calorimetric study

The DSC curve for $[(C_3H_7)_4P]_2Cd_2Br_6$ crystals recorded on heating between 300 and 440 K with a scanning rate (5.00 °C/min) is shown in Fig. 3. This thermogram reveals the presence of one endothermic peak located at 364 K. This anomaly is may be due to a phase transition.

The transition enthalpy and entropy determined for the first peak are 2.62 kJ mol⁻¹ and 7.19 J mol⁻¹ K⁻¹, respectively. The mechanism experimentally observed in transition entropies can be

interpreted in terms of Boltzmann's principle $\Delta S = R \ln \Omega$ [16]. The ΔS relation of transition brings about a number of equivalent positions $\Omega = 2.4$, which implies that the $[(C_3H_7)_4P]^+$ and/or the anionic parts acquire quite a large part of their motional freedom at phase transition [17,18]. The entropy value of the transition is large than $R \ln 2$, so the phase transition at $T = 364$ K can be classified as an order-disorder [19]. This transition ($T = 364$ K), is similar to those observed in other compounds of tetraalkylphosphonium groups [20-22]. The order of the phase transition can be determined from the shape of the peaks. If the peak is strong, it exhibits the characteristics of a first-order transition. In contrast, when the peaks are very weak, they can be corresponding to a second-order transition [23]. For the $[(C_3H_7)_4P]_2Cd_2Br_6$ crystal, The peak at 364 K is very strong, so the transition is of the first order.

3. Electrical properties

3.1. Nyquist plots

The electrical properties have been studied by complex impedance spectroscopy over a range of frequency and temperature. The method ensures separation of the bulk, grain boundary and electrode properties, giving an insight about the electrical processes, taking place within the system and their correlation with sample microstructure, when modeled in terms of their equivalent electrical circuit.

The complex impedance spectra (Z'' versus Z') of the $[(C_3H_7)_4P]_2Cd_2Br_6$ compound obtained at different temperatures (Fig. 4).

The radius semicircles decreases with the increase of temperature as well as the centers of these semicircles are located below the real axis, which indicates the non-ideal Debye behavior [24]. In order to study the electric properties of this compound, we proposed an equivalent circuit model (inset in Fig. 4) formed by the parallel combination of the apparent resistance (R), the capacitance (C) and fractal capacitance (CPE).

The experimental values of Z' and $-Z''$ as a function of the angular frequency are given in Fig. 5 (a) and (b) respectively. The good conformity of the experimental data with calculated lines indicating that the suggested equivalent circuit describes well the electrical properties of the sample.

3.2. DC conductivity

The values of the extracted circuit parameters are used to calculate the DC electrical conductivity σ_{dc} of the sample expressed by the following relation:

$$\sigma_{dc} = d/S * R \quad (1)$$

where R is the value of the resistance, S is the area of the sample and d is the thickness sample. The temperature dependence of the conductivity $\ln(\sigma_{dc} * T)$ versus $(1000/T)$ in the studied temperature range is given in Fig. 6. Two straight-lines with distinct slopes are observed, around $T=364$ K, which is in concordance with thermal analysis results (Fig.3). Arrhenius behavior is observed in the regions I and II, which is given by the following relation [25]:

$$\sigma_{dc} * T = A \exp(-E_a / K_B * T) \quad (2)$$

where A is the pre-exponential factor, E_a is the activation energy and K_B is the Boltzmann constant. The calculated activation energies obtained by the linear fit are equal to: $E_a(I) = 0.55$ eV and $E_a(II) = 0.78$ eV. The change of the activation energies at low and high temperature region can be explained by the change in motions of anionic and cationic parts with temperature.

3.3. AC conductivity

The temperature dependence of the calculated total electrical conductivity (σ) at different frequency can be defined by the Jonscher universal power law [26]:

$$\sigma_{ac} = \sigma_{dc} + A\omega^s \quad (3)$$

where ω the angular frequency, σ_{ac} is the conductivity in alternative current, σ_{dc} is the conductivity in continuous current, A is a constant for a particular temperature and S is an exponent dependent on frequency and temperature which is used to suggest the appropriate model for the conduction mechanism. Fig. 7 shows the frequency dependence AC conductivity at different temperatures. At high frequencies, the conductivity shows dispersion pattern, which shifts toward higher frequency with increasing temperature, attributes to the AC conductivity. Whereas the frequency independent plateau region at low frequencies corresponds to DC conductivity of the material. For each temperature the high and low frequency regions are separated by a change in slope at a certain value of frequency. This frequency is known as the hopping frequency [27]. It is seen that the plateau region of the D.C conductivity increases and extends towards high frequencies as the temperature increased which indicates that the charge carriers can move easily towards the high frequencies.

The hopping frequency ω_h of the charge carriers can be calculated from AC conductivity data using the formula [22]:

$$\omega_h = (\sigma_{dc}/A)^{1/S} \quad (4)$$

We have plotted in Fig. 8 the variation of $\ln(\omega_h)$ as a function of $1000/T$. This curve shows the appearance of Arrhenius behavior. The activation energies calculated from straight line

are equal to 0.54 eV (I) and 1.04 eV (II) for low and high temperature region respectively. It is appeared that the calculated activation energies (E_a) are very close to those obtained from DC conductivity, which suggest that the mobility of the charge carriers is due to the hopping mechanism [29].

In literature various models have been proposed to correlate the conduction mechanism of AC conductivity with $S(T)$ behavior [30-32]. The variation of the exponent S with the temperature of $[(C_3H_7)_4P]_2Cd_2Br_6$ crystal is depicted in Fig. 9. It is clear from this figure that the exponent S decrease with the increasing of temperatures. Therefore, the correlate barrier model (CBH) accords well with the results obtained.

Figure 10 shows the shape of $\text{Log}(\sigma_{ac}/\sigma_{dc})$ as a function of $\text{Log}(\omega/\omega_h)$ of the title compound for several temperatures. Various formalisms are used to characterize the conductivity between them, we use th Ghosh model [33]:

$$\sigma_{ac}(\omega)/\sigma_{dc} = F(\omega/\omega_h) \quad (5)$$

As we can notice that the conductivity spectrum increases with increasing temperature. This behavior indicates that the relaxation mechanism of charge carriers is independent of temperature [34].

3.4. Modulus discussion

The electric modulus formalism is an important theory formulated by Macedo et al. [35, 36]. This formalism permits to study charge transport processes such as the mechanism of electrical transport, conductivity relaxation and ion dynamics as a function of frequency and temperature in ion conductors. It also suppresses the effect of the electrode polarization and/or mobile ion polarization.

Figure 11 represents the variation of imaginary part M'' with the angular frequency at different temperatures. It is clearly that M'' exhibits a single relaxation peak associated with the grain effect, which confirms the observed result in the impedance spectra. This peak shifts towards higher frequencies with increasing in temperature, indicating the correlation between motions of mobile ions charges [37]. In other part, this figure indicates that the theoretical calculation fit agrees well with the experimental data.

3.5. *Temperature and Frequency dependence of the Dielectric Loss ϵ''*

The variation of the imaginary part ϵ'' with temperature and frequency for $[(C_3H_7)_4P]_2Cd_2Br_6$ material is illustrated in Figs. 12 and 13. It is clear that ϵ'' is temperature independent up to about 363 K and then it increases with increasing temperature. This variation owing to the dipole orientation and the higher charge carrier density contribution at high temperatures [38, 39]. The dielectric loss decreases with increasing frequency, this decrease can be attributed to the migration of ions in the material at lower frequencies. Accordingly, the dielectric loss at low frequencies is characterized by high values of ϵ'' due to the contribution of ion jump and conduction loss. However, at higher frequencies, the ion vibrations may be the only source of dielectric loss and so ϵ'' decrease at higher values of frequency.

4. Conclusion

The present work was dedicated for the synthesis, crystal structure, differential scanning calorimetry, electrical and dielectric properties of the bis-tetrapropylphosphonium hexabromo-dicadmate, $[(C_3H_7)_4P]_2Cd_2Br_6$. The atomic arrangement could be described by an alternation of organic and inorganic layers along the [100] direction. The two entities in this compound were interconnected by van der Waals and electrostatic interactions. The

differential scanning calorimetry revealed one phase transition at 364 K, from phase I to phase II, which was suggested as an order–disorder type. Impedance spectroscopy was used to characterize the electrical and dielectrical behavior of this material as a function of frequency at various temperatures. Besides, from the Nyquist plots, it was shown that this compound modeled by the simple equivalent circuit, formed by the parallel combination of a resistance (R), a capacitance (C) and a fractal capacitance (CPE). The study of DC conductivity showed Arrhenius behavior in two straight-lines regions (I) and (II) and the calculated activation energies were E_a (I) = 0.55 eV and E_a (II) = 0.78 eV respectively. The thermal behavior of the extracted exponent S confirmed that the CBH model is the appropriate model for this compound. Dielectric measurements revealed that the dielectric loss decreased with increasing frequencies and raised with increasing temperatures.

References

1. M. Khalfa, A. Oueslati, K. Khirouni, M. Gargouri, A. Rousseau, J. Lhoste, J.-F. Bardeau and G. Corbel, *RSC Advances* **12** (2022) 2798.
2. A. Mhiri, F. Krichen, A. Oueslati, J. Lhoste, F. Goutenoire, M. Gargouri, A. Bulou, J. *Alloys and Compounds* **772** (2019) 546.
3. A. Oueslati, M. Gargouri, J. *Alloys and Compounds* **739** (2018) 1089.
4. M. Szafranski, *Crystal Growth & Design* **16** (2016) 3771.
5. M. Wojtaś, W. Medycki, J. Baran, R. Jakubas, *Chemical Physics* **371** (2010) 66.
6. H. Elgahami, W. Trigui, A. Oueslati, F. Hlel, J. *Ionics* **25** (2019) 1359.
7. M. Ines, M. Ben Gzaiel, A. Oueslati, S. Auguste, J. Lhoste, M. Gargouri, J. *Molecular Structure* **1226** (2010) 129361.

8. A. Ben Rhaiem, F. Hlel, K. Guidara, M. Gargouri, J. Spectrochimica Acta Part A **66** (2007) 1107.
9. M. Wojtaś, R. Jakubas, Z. Ciunik, W. Medycki, J. Solid State Chemistry **177** (2004) 1575.
10. W. Trigui, A. Oueslati, I. Chaabane, F. Hlel, J. Ionics **4** (2014) 231.
11. H. Elgahami, W. Trigui, A. Oueslati, J. Lhoste, F. Hlel, Applied Organometallic chemistry **33** (2019) e5078.
12. M. Ben Gzaïel, A. Oueslati, J. Lhoste, M. Gargouri, A. Bulou, J. Molecular Structure **1089** (2015) 153.
13. A. Oueslati, F. Hlel, M. Gargouri, Ionics **17** (2011) 91.
14. G. M. Sheldrick, J. Acta Crystallographica A **71** (2015) 3.
15. G. M. Sheldrick, J. Acta Crystallographica C **71** (2015) 3.
16. W.H. Baur, J. Acta Crystallographica Section B **30** (1974) 1195.
17. S. Hajlaoui, I. Chaabane, A. Oueslati, K. Guidara, J. Solid State Sciences **25** (2013) 134.
18. W. Trigui, A. Oueslati, I. Chaabane, F. Hlel, J. Solid State Chemistry **227** (2015) 10.
19. R. Decressain, R. Jakubas, G. Bator, J. Zaleski, J. Lefebvre, J. Kusz, J. Physics and Chemistry of Solids **59** (1998) 1487.
20. N. Weslati, I. Chaabane, A. Bulou, F. Hlel, J. Physica B **441** (2014) 42.
21. N. Hannachi, K. Guidara, A. Bulou, F. Hlel, J. Materials Research Bulletin **45** (2010) 1754.
22. A. Ben Rhaiem, F. Hlel, K. Guidara, M. Gargouri, J. Spectrochimica Acta Part A **66** (2007) 1107.
23. C. Ben Mohamed, K. Karoui, F. jomni, K. Guidara, A. Ben Rhaiem, J. Molecular Structure **1082** (2015) 38.
24. B. Louati, K. Guidara, J. Materials Sciences and Engineering **177** (2012) 838.

25. K.S. Rao, P.M. Krishna, D.M. Prasad, J.H. Lee, J.S. Kim, J. Alloys and Compounds **464** (2008) 497.
26. A.K. Jonscher, J. Nature **276** (1977) 673.
27. H. Nefzi, F. Sediri, H. Hamzaoui, N. Gharbi, J. Materials Research Bulletin **48** (2013) 1978.
28. S. Nasri, M. Megdiche, M. Gargouri, K. Guidara, J. Ionics **20** (2014) 399.
29. S. Nasri, M. Megdiche, K. Guidara, M. Gargouri, J. Ionics **19** (2013) 1921.
30. A. Ghosh, J. Physical Review B, **41** (1990) 1479.
31. M. Pollak, J. Philosophical Magazine, **23** (1971) 519.
32. A. Ghosh, J. Physical Review B, **42** (1990) 5665.
33. B. Roling, A. Happe, K. Funke, M.D. Ingram, J. Physical Review Letters, (1997) **78**, 2160.
34. A. Pan, A. Ghosh, J. Physical Review B, **66** (2002) 1.
35. P. S. Anantha, K. Harihanan, J. Materials Science and Engineering: B, **121** (2005) 12.
36. P. B. Macedo, C.T. Moynihan, R. Bose, J. Physics and Chemistry of Glasses, **13** (1972) 171.
37. S. Sahoo, U. Dash, S. K. S. Parashar, S. M. All, J. Advanced Ceramics, **2** (2013) 291.
38. A. Oueslati, F. Hlel, K. Guidara, and M. Gargouri, J. Alloys and Compounds, **492** (2010) 508.
39. F. Alvarez, A. Alegri, J. Colmenero, J. Physical Review B **47**, 125 (1993).

Table 1 : Parameters of data collection, and results of structure refinement for $[(C_3H_7)_4P]_2Cd_2Br_6$.

Crystal data	
Chemical formula	$2(C_{12}H_{28}P)Cd_2Br_6$
Crystal color	colourless
Crystal description	prism
Molecular weight ($g \cdot mol^{-1}$)	1110.88
Crystal system, space group	Triclinic, <i>P</i> -1
Temperature (K)	150
a, b, c (Å)	13.662(3), 16.146(4), 16.857(4)
α, β, γ (°)	114.867(6), 91.650(8), 114.357(7)
V (Å ³)	2980.1 (12)
Z	3
Radiation type	Mo K_α
μ (mm^{-1})	7.197
No. of measured, independent and observed [$I > 2\sigma(I)$] reflections	16394, 3573, 2997
R_{int}	0.075
D_{cal} ($Mg \cdot m^{-3}$)	1.857
$R[F^2 > 2\sigma(F^2)], wR(F^2), S$	0.087, 0.242, 1.09
No. of reflections	3573
No. of parameters	264
$\Delta\rho_{max}, \Delta\rho_{min}$ ($e \cdot \text{Å}^{-3}$)	1.42, -1.01
θ range for data collection (°)	1.52-27.73
$F(000)$	1608
Range of $h \ k \ l$	$h = -11 \rightarrow 11$ $k = -13 \rightarrow 13$ $l = -14 \rightarrow 14$

Table 2: Atomic coordinates and equivalent thermal agitation factors in the $[(C_3H_7)_4P]_2Cd_2Br_6$ compound.

	<i>x</i>	<i>y</i>	<i>z</i>	U_{iso}/U_{eq}
P1	0.335 (1)	0.167 (8)	0.574 (7)	0.025 (3)
C1	0.228 (4)	0.147 (3)	0.631 (3)	0.044 (4)
H1A	0.157	0.100	0.587	0.052
H1B	0.236	0.115	0.666	0.052
C2	0.227 (4)	0.248 (3)	0.693 (3)	0.044 (4)
H2A	0.202	0.273	0.657	0.052
H2B	0.300	0.300	0.730	0.052
C3	0.145 (4)	0.228 (3)	0.755 (3)	0.044 (4)
H3A	0.143	0.290	0.794	0.065
H3B	0.071	0.176	0.718	0.065
H3C	0.169	0.203	0.791	0.065
C4	0.468 (4)	0.226 (3)	0.651 (3)	0.044 (4)
H4A	0.525	0.244	0.619	0.052
H4B	0.477	0.289	0.701	0.052
C5	0.486 (4)	0.165 (3)	0.687 (3)	0.044 (4)
H5A	0.471	0.099	0.637	0.052
H5B	0.432	0.151	0.723	0.052
C6	0.602 (4)	0.216 (3)	0.746 (3)	0.044 (4)
H6A	0.606	0.170	0.767	0.065
H6B	0.655	0.227	0.711	0.065
H6C	0.616	0.280	0.796	0.065
C7	0.337 (4)	0.248 (3)	0.528 (3)	0.044 (4)
H7A	0.263	0.217	0.491	0.052
H7B	0.352	0.314	0.577	0.052
C8	0.418 (4)	0.265 (3)	0.473 (3)	0.044 (4)
H8A	0.402	0.198389	0.423156	0.052
H8B	0.492	0.294	0.509	0.052
C9	0.417 (4)	0.337 (3)	0.434 (3)	0.044 (4)
H9A	0.470	0.345	0.399	0.065
H9B	0.344	0.307	0.396	0.065
H9C	0.433	0.403	0.483	0.065
C10	0.306 (4)	0.042 (3)	0.485 (3)	0.044 (4)
H10A	0.371	0.048	0.461	0.052
H10B	0.291	-0.004	0.509	0.052
C11	0.209 (4)	-0.004 (3)	0.408 (3)	0.044 (4)
H11A	0.145	-0.003	0.430	0.052
H11B	0.227	0.036	0.376	0.052
C12	0.184 (4)	-0.113 (3)	0.344 (3)	0.044 (4)
H12A	0.122	-0.142	0.294	0.065
H12B	0.247	-0.113	0.321	0.065
H12C	0.165	-0.153	0.375	0.065
P2	0.979 (1)	0.4756 (8)	0.736 (8)	0.028 (3)
C21	0.899 (4)	0.398 (3)	0.785 (3)	0.041 (4)
H21A	0.845	0.420	0.807	0.049
H21B	0.857	0.326	0.736	0.049

C22	0.965 (4)	0.398 (3)	0.862 (3)	0.041 (4)
H22A	1.016	0.372	0.838	0.049
H22B	1.008	0.468	0.909	0.049
C23	0.893 (4)	0.335 (3)	0.900 (3)	0.041 (4)
H23A	0.937	0.338	0.947	0.062
H23B	0.842	0.361	0.924	0.062
H23C	0.850	0.264	0.853	0.062
C24	1.071 (4)	0.435 (3)	0.690 (3)	0.041 (4)
H24A	1.106	0.425	0.733	0.049
H24B	1.027	0.367	0.638	0.049
C25	1.159 (4)	0.495 (3)	0.659 (3)	0.041 (4)
H25A	1.206	0.561	0.711	0.049
H25B	1.124	0.509	0.618	0.049
C26	1.234 (4)	0.453 (3)	0.612 (3)	0.041 (4)
H26A	1.286	0.502	0.596	0.062
H26B	1.272880	0.441951	0.651727	0.062
H26C	1.190	0.389	0.558	0.062
C27	1.055 (4)	0.605 (3)	0.830 (3)	0.041 (4)
H27A	1.006	0.615	0.870	0.049
H27B	1.117	0.609	0.862	0.049
C28	1.099 (4)	0.695 (3)	0.806 (3)	0.041 (4)
H28A	1.148	0.686	0.766	0.049
H28B	1.036	0.692	0.772	0.049
C29	1.159 (4)	0.799 (3)	0.888 (3)	0.041 (4)
H29A	1.184	0.851	0.870	0.062
H29B	1.109	0.807	0.926	0.062
H29C	1.220	0.802	0.920	0.062
C30	0.894 (4)	0.469 (4)	0.649 (3)	0.041 (4)
H30A	0.941	0.511	0.624	0.049
H30B	0.856	0.398	0.601	0.049
C31	0.804 (4)	0.504 (3)	0.678 (3)	0.041 (4)
H31A	0.838	0.573	0.728	0.049
H31B	0.750	0.457	0.696	0.049
C32	0.744 (4)	0.502 (3)	0.595 (3)	0.041 (4)
H32A	0.688	0.523	0.612	0.062
H32B	0.797	0.547	0.577	0.062
H32C	0.709	0.432	0.545	0.062
P3	0.318 (1)	0.182 (8)	0.072 (8)	0.029 (3)
C41	0.395 (4)	0.322 (3)	0.126 (3)	0.041 (4)
H41A	0.472	0.340	0.127	0.049
H41B	0.371	0.344	0.087	0.049
C42	0.385 (4)	0.378 (3)	0.216 (3)	0.041 (4)
H42A	0.404	0.352	0.254	0.049
H42B	0.309	0.365	0.214	0.049
C43	0.462 (4)	0.493 (3)	0.256 (3)	0.041 (4)
H43A	0.453	0.528	0.315	0.061
H43B	0.536	0.505	0.258	0.061
H43C	0.442	0.518	0.218	0.061
C44	0.372 (4)	0.129 (4)	-0.016 (3)	0.041 (4)
H44A	0.323	0.054	-0.048	0.049

H44B	0.369	0.155	-0.057	0.049
C45	0.490 (4)	0.148 (4)	0.010 (3)	0.041 (4)
H45A	0.491	0.113	0.046	0.049
H45B	0.538	0.221	0.047	0.049
C46	0.537 (4)	0.107 (3)	-0.072 (3)	0.041 (4)
H46A	0.610	0.120	-0.052	0.061
H46B	0.490	0.033	-0.108	0.061
H46C	0.537	0.140	-0.107	0.061
C47	0.177 (4)	0.144 (4)	0.027 (3)	0.041 (4)
H47A	0.131	0.074	0.017	0.049
H47B	0.154	0.189	0.072	0.049
C48	0.154 (4)	0.146 (4)	-0.059 (3)	0.041 (4)
H48A	0.165	0.094	-0.106	0.049
H48B	0.204	0.213	-0.052	0.049
C49	0.036 (4)	0.127 (3)	-0.083 (3)	0.041 (4)
H49A	0.023	0.128	-0.138	0.061
H49B	-0.014	0.059	-0.090	0.061
H49C	0.024	0.178	-0.036	0.061
C50	0.323 (4)	0.138 (3)	0.150 (3)	0.041 (4)
H50A	0.399	0.169	0.181	0.049
H50B	0.283	0.162	0.194	0.049
C51	0.274 (4)	0.023 (3)	0.112 (3)	0.041 (4)
H51A	0.315	-0.001	0.070	0.049
H51B	0.197	-0.009	0.077	0.049
C52	0.275 (4)	-0.009 (3)	0.185 (3)	0.041 (4)
H52A	0.243	-0.082	0.157	0.061
H52B	0.350	0.022	0.217	0.061
H52C	0.233	0.014	0.225	0.061
Cd1	0.640 (3)	0.505 (3)	1.013 (2)	0.0347 (1)
Br1	0.698 (4)	0.447 (4)	1.116 (4)	0.0502 (2)
Br2	0.781 (5)	0.565 (4)	0.931 (4)	0.0519 (2)
Br3	0.437 (4)	0.359 (3)	0.909 (3)	0.0338 (1)
Cd11	-0.283 (3)	0.192 (3)	0.368 (2)	0.0339 (1)
Cd12	-0.029 (3)	0.168 (3)	0.355 (2)	0.0351 (1)
Br11	-0.349 (5)	0.172 (4)	0.5000 (4)	0.0510 (2)
Br12	-0.388 (5)	0.226 (4)	0.271 (4)	0.0609 (2)
Br13	-0.241 (4)	0.037 (3)	0.266 (3)	0.0353 (1)
Br14	-0.067 (4)	0.330 (3)	0.429 (3)	0.0326 (1)
Br15	0.011 (4)	0.131 (4)	0.481 (3)	0.0493 (2)
Br16	0.093 (5)	0.184 (4)	0.250 (4)	0.062 (2)

Table 3 : Bond lengths d (Å) and angles (deg) for [(C₃H₇)₄P]₂Cd₂Br₆.

Lengths	d (Å)	Angles	(deg)
P1—C7	1.77 (4)	C7—P1—C1	110 (2)
P1—C1	1.77 (5)	C7—P1—C4	109 (2)
P1—C4	1.80 (5)	C1—P1—C4	111 (2)
P1—C10	1.80 (4)	C7—P1—C10	109 (2)
C1—C2	1.52 (6)	C1—P1—C10	107 (2)
C30—C31	1.56 (6)	C4—P1—C10	111 (2)
C2—C3	1.59 (6)	C2—C1—P1	112 (3)
C31—C32	1.57 (6)	C31—C30—P2	116(3)
C4—C5	1.45(6)	C1—C2—C3	109 (3)
P3—C44	1.73 (4)	C30—C31—C32	109 (3)
P3—C50	1.74 (4)	C5—C4—P1	117 (3)
C5—C6	1.53 (6)	C44—P3—C50	110 (2)
P3—C41	1.81 (4)	C44—P3—C41	110 (2)
P3—C47	1.80 (5)	C4—C5—C6	115 (4)
C41—C42	1.46 (5)	C50—P3—C41	111 (2)
C42—C43	1.52 (6)	C29—C28—C27	112 (3)
C7—C8	1.49 (6)	C44—P3—C47	108 (2)
C8—C9	1.57 (6)	C50—P3—C47	109 (2)
C44—C45	1.53 (6)	C41—P3—C47	108 (2)
C45—C46	1.55 (6)	C42—C41—P3	117 (3)
C10—C11	1.50 (6)	C43—C42—C41	111 (4)
C11—C12	1.50 (6)	C8—C7—P1	116 (3)
C47—C48	1.50 (6)	C7—C8—C9	113 (4)
C48—C49	1.51 (6)	C45—C44—P3	116 (3)
P2—C24	1.70 (5)	C46—C45—C44	112 (3)
P2—C21	1.80 (4)	C11—C10—P1	115 (2)
P2—C27	1.81 (4)	C48—C47—P3	116 (3)
P2—C30	1.79 (5)	C49—C48—C47	111 (4)
C21—C22	1.56 (6)	C24—P2—C21	111 (2)
C50—C51	1.53 (4)	C24—P2—C27	110 (2)
C22—C23	1.52 (4)	C21—P2—C27	105 (2)
C51—C52	1.50 (5)	C24—P2—C30	107 (2)
C24—C25	1.47 (6)	C21—P2—C30	112 (2)
C25—C26	1.52 (6)	C27—P2—C30	113(2)
C27—C28	1.56 (6)	C22—C21—P2	116 (3)
C28—C29	1.49 (5)	C51—C50—P3	116 (3)
Cd1—Br2	2.515 (6)	C23—C22—C21	113 (4)
Cd1—Br1	2.525 (6)	C52—C51—C50	112 (3)
Cd1—Br3 ⁱ	2.676 (6)	C25—C24—P2	122 (3)
Cd1—Br3	2.677 (6)	C28—C27—P2	116 (3)
Cd11—Br12	2.518 (6)	C24—C25—C26	120 (4)
Cd12—Br13	2.673(6)	Br2—Cd1—Br1	114.6 (2)
Cd12—Br14	2.664 (6)	Br2—Cd1—Br3	115.1 (2)
Cd12—Br15	2.535 (6)	Br1—Cd1—Br3	108.6 (2)
Cd12—Br16	2.504 (6)	Br2—Cd1—Br3 ⁱ	111 (2)
Cd11—Br14	2.678 (6)	Br1—Cd1—Br3 ⁱ	114.7 (2)
Cd11—Br13	2.670 (6)	Br3—Cd1—Br3 ⁱ	90.6 (2)

Cd11—Br11	2.515 (6)	Br12—Cd11—Br11	120 (2)
		Br12—Cd11—Br13	110.5 (2)
		Br11—Cd11—Br13	110.6 (2)
		Br12—Cd11—Br14	112.3 (2)
		Br11—Cd11—Br14	107.4 (2)
		Br13—Cd11—Br14	92.6 (2)
		Br16—Cd12—Br15	122.4 (2)
		Br16—Cd12—Br14	111 (2)
		Br15—Cd12—Br14	106.9 (2)
		Br16—Cd12—Br13	111.5 (2)
		Br15—Cd12—Br13	107.9 (2)
		Br14—Cd12—Br13	92.9 (2)

Journal Pre-proof

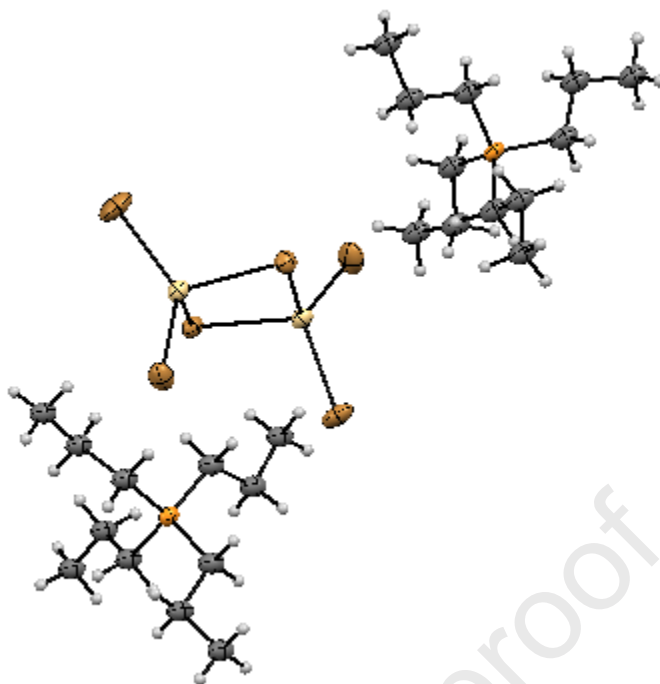


Figure 1 : crystal structure of the $[(C_3H_7)_4P]_2Cd_2Br_6$ compound.

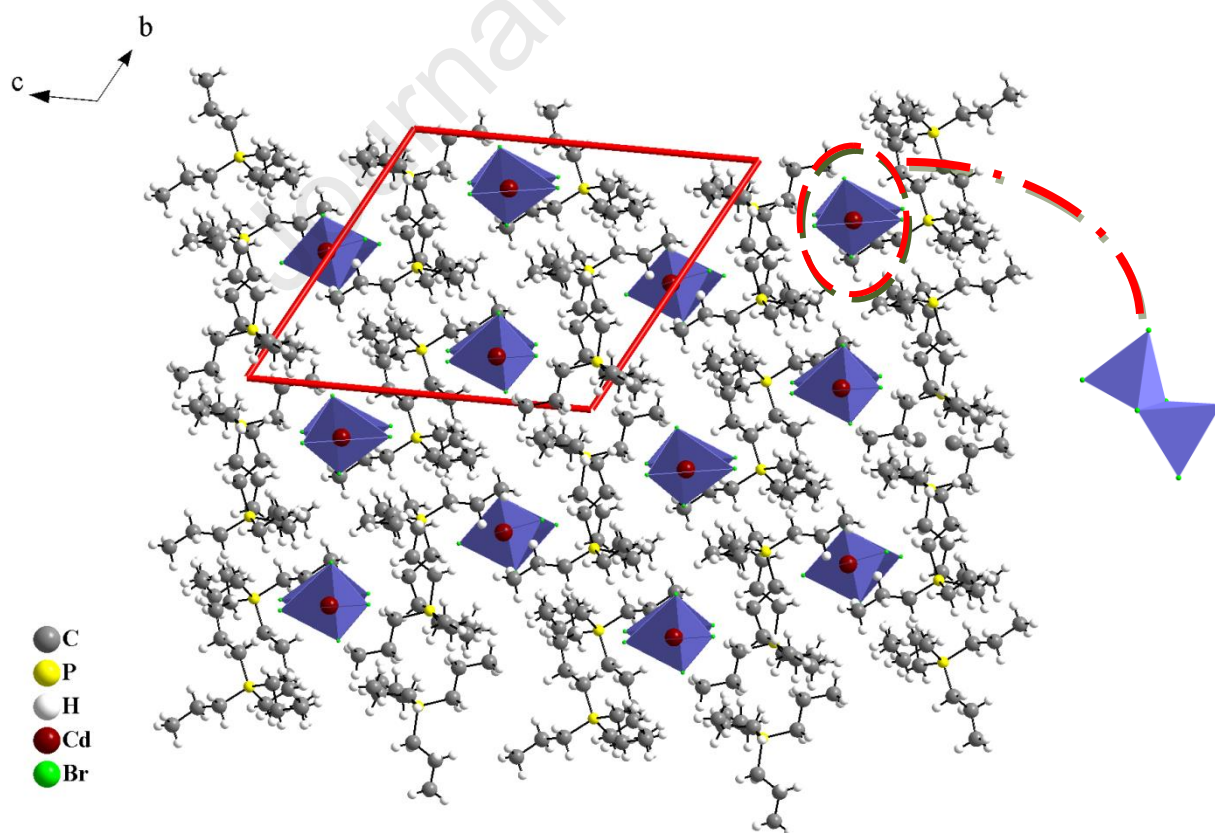


Figure 2 : Projection along the a axis of the atomic arrangement of $[(C_3H_7)_4P]_2Cd_2Br_6$.

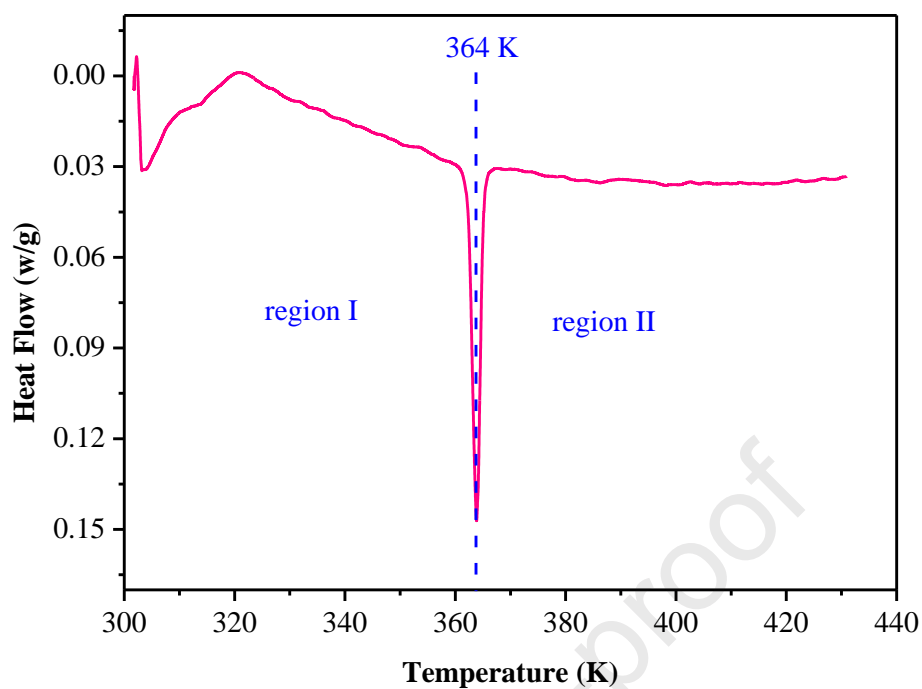


Figure 3 : Differential scanning calorimetric of $[(C_3H_7)_4P]_2Cd_2Br_6$.

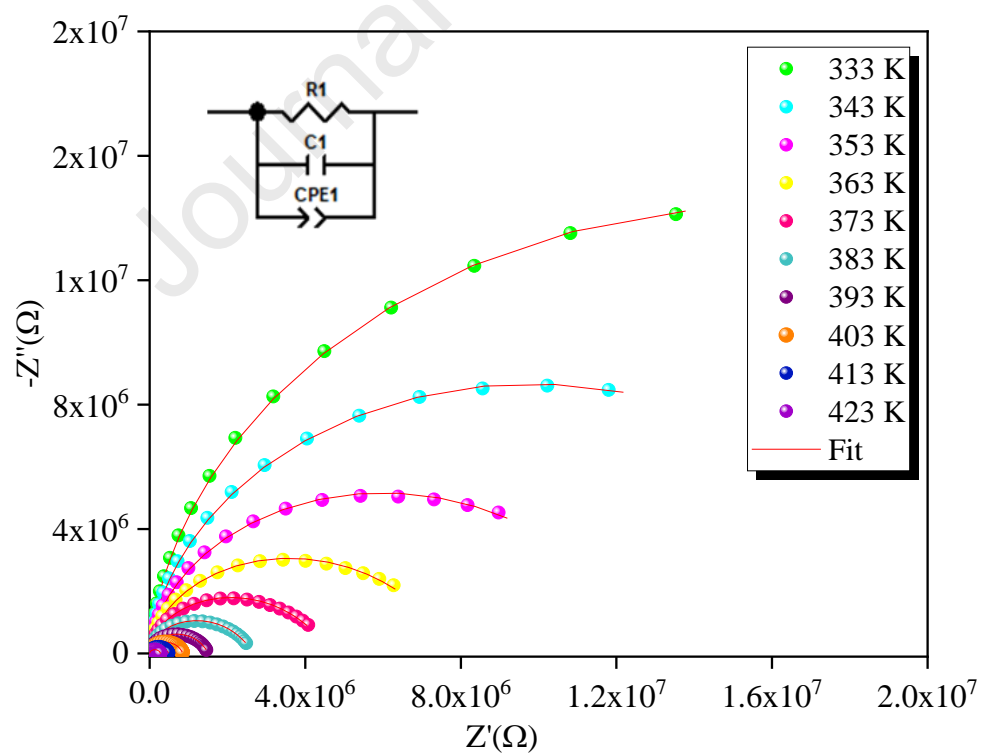


Figure 4 : Observed and calculated impedance complex plane plots of the $[(C_3H_7)_4P]_2Cd_2Br_6$ compound.

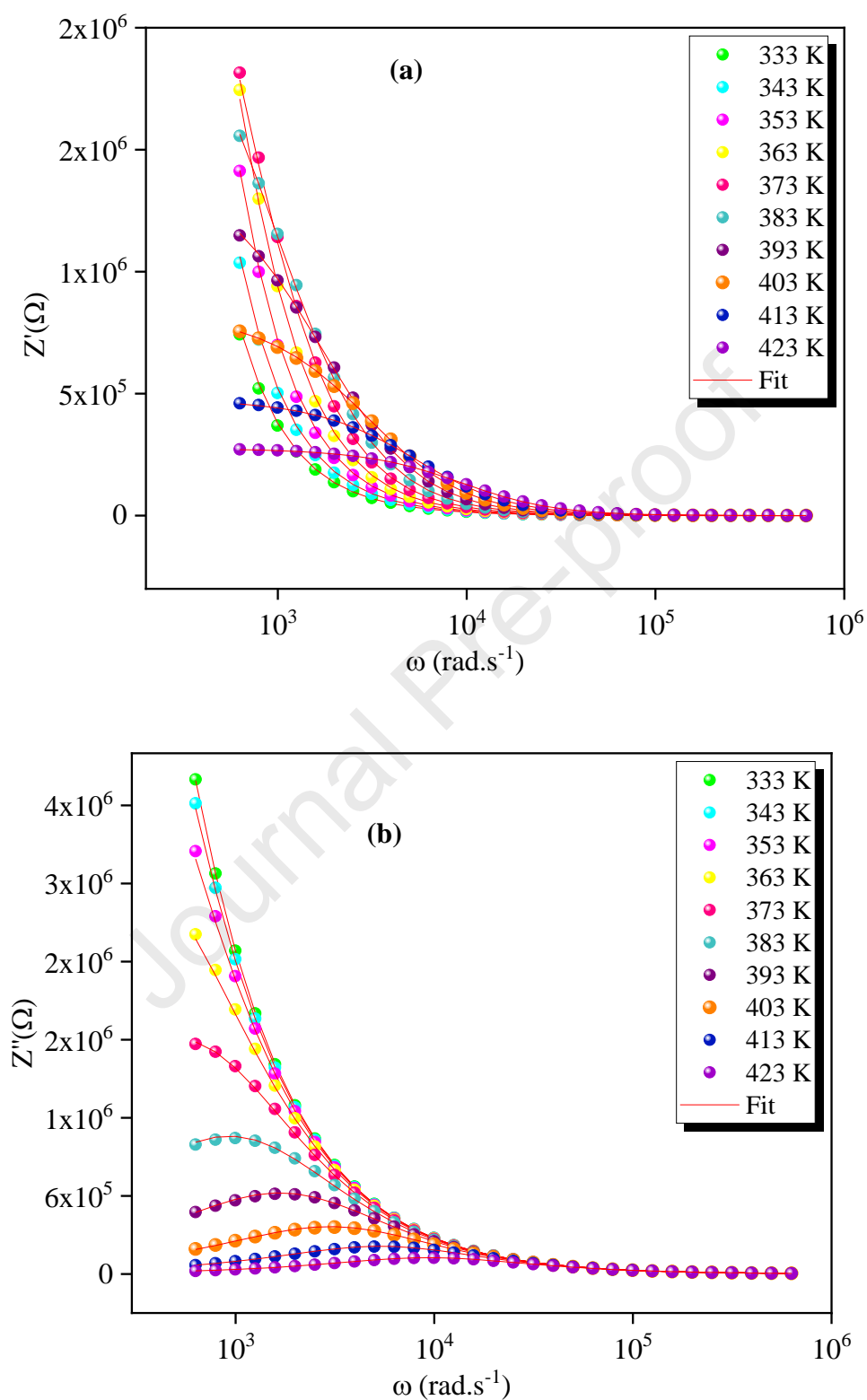


Figure 5 : Frequency dependence of $Z'(\omega)$ (a) and $-Z''(\omega)$ (b) at various temperatures of

$[(C_3H_7)_4P]_2Cd_2Br_6$ compound.

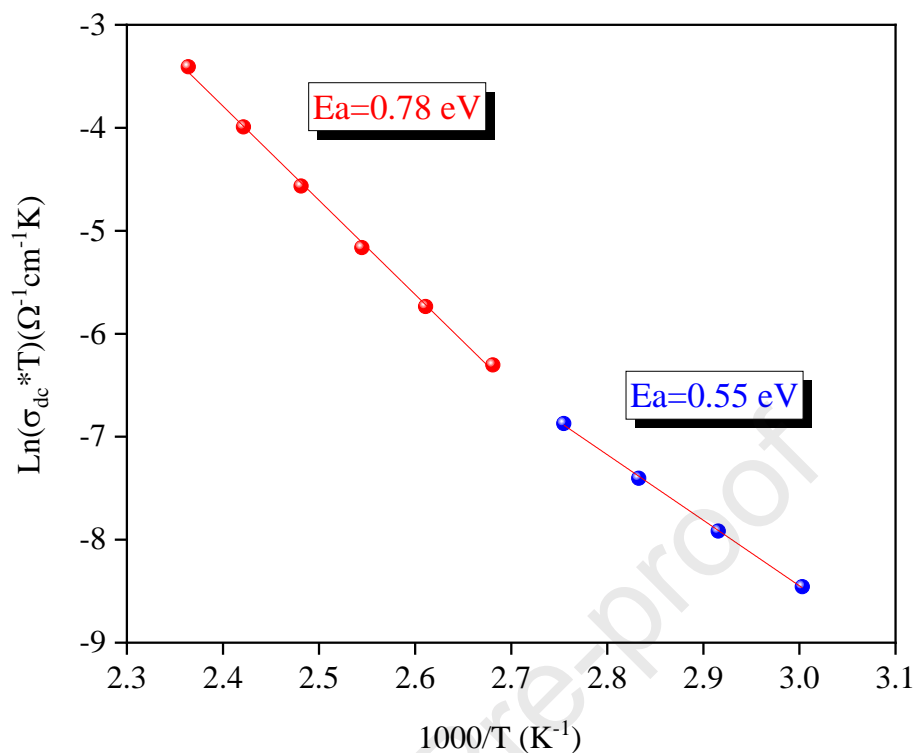


Figure 6 : Arrhenius relation of $\text{Ln}(\sigma_{\text{dc}} * T)$ versus $1000/T$ for $[(\text{C}_3\text{H}_7)_4\text{P}]_2\text{Cd}_2\text{Br}_6$.

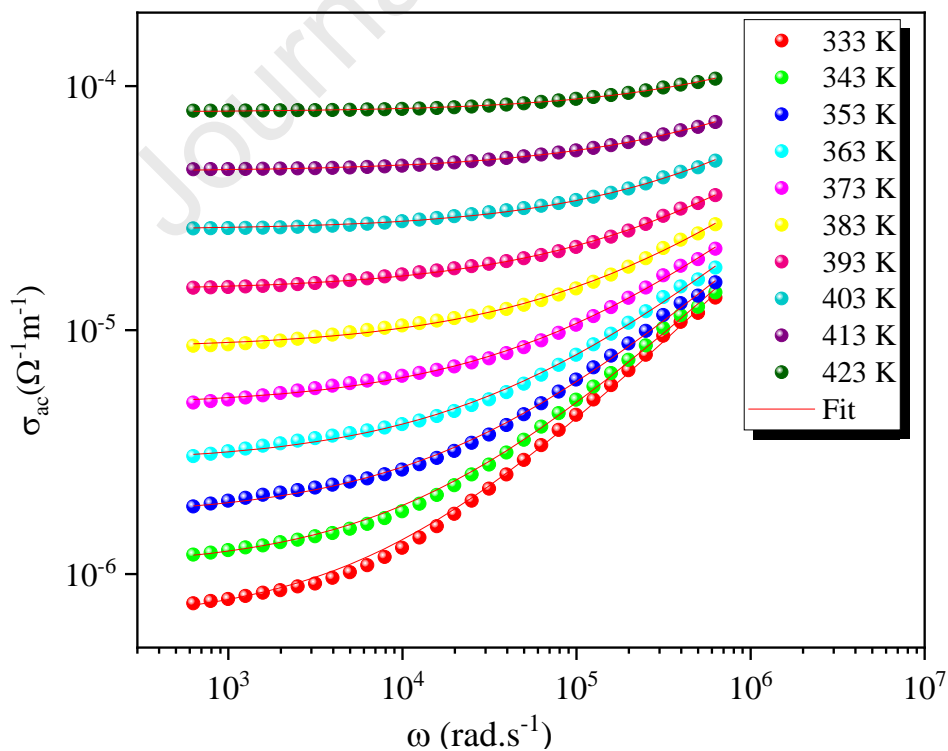


Figure 7 : Dependence of ac conductivity with the angular frequency at different temperatures.

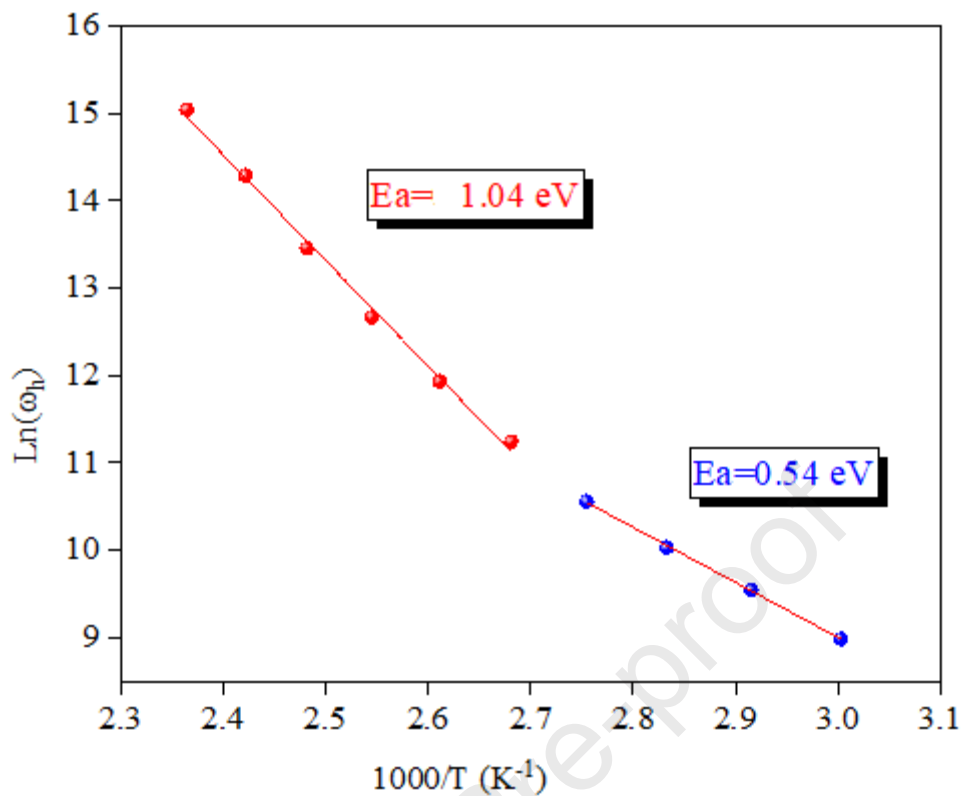


Figure 8 : Temperature dependence of hopping frequency ω_h .

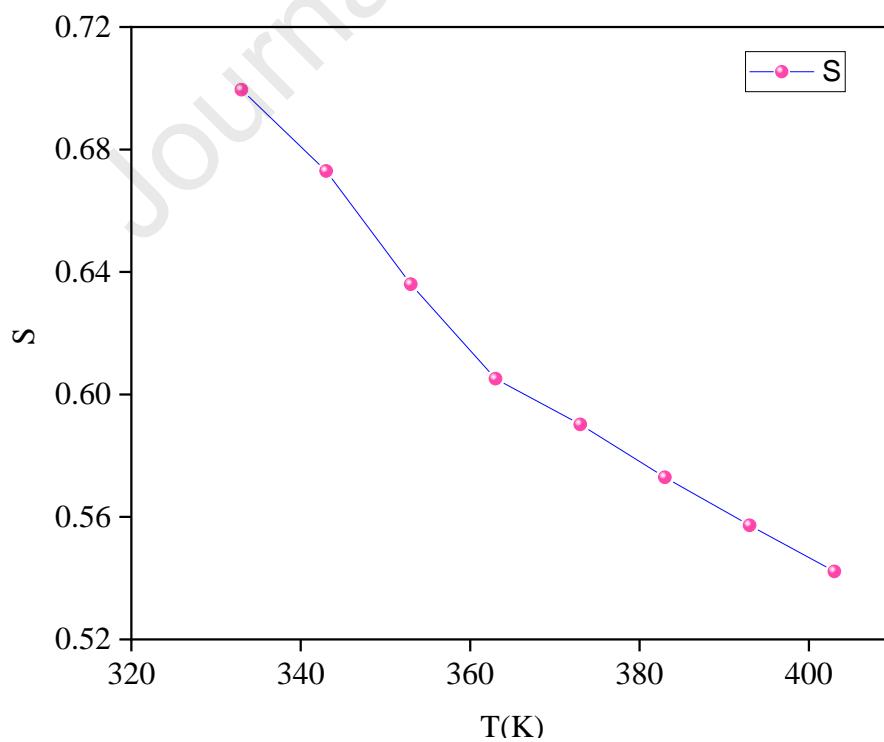


Figure 9 : Temperature dependence of the exponent S for the $[(\text{C}_3\text{H}_7)_4\text{P}]_2\text{Cd}_2\text{Br}_6$ compound.

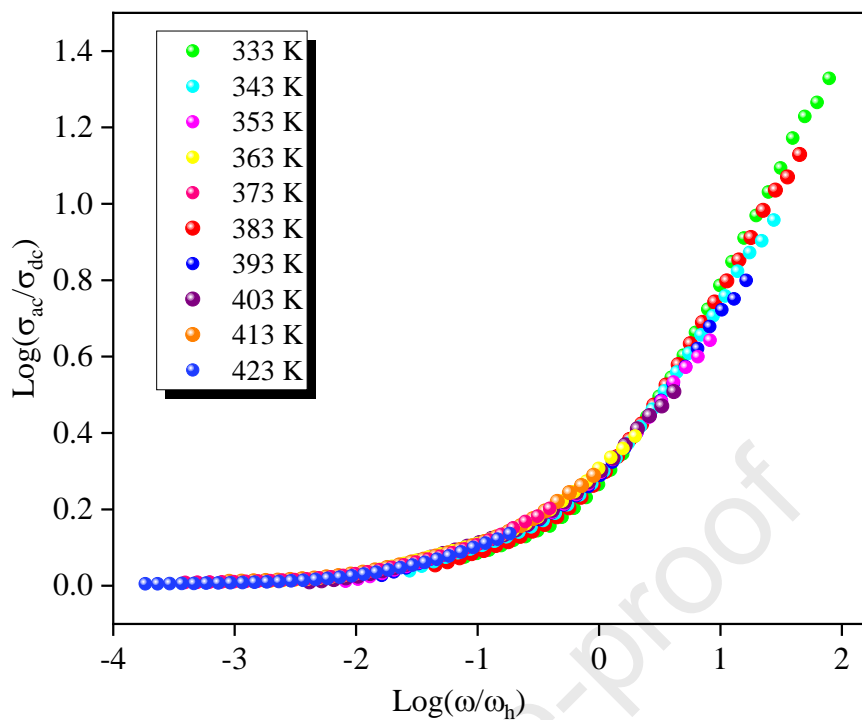


Figure 10 : Conductivity master plot at several temperatures for $[(C_3H_7)_4P]_2Cd_2Br_6$.

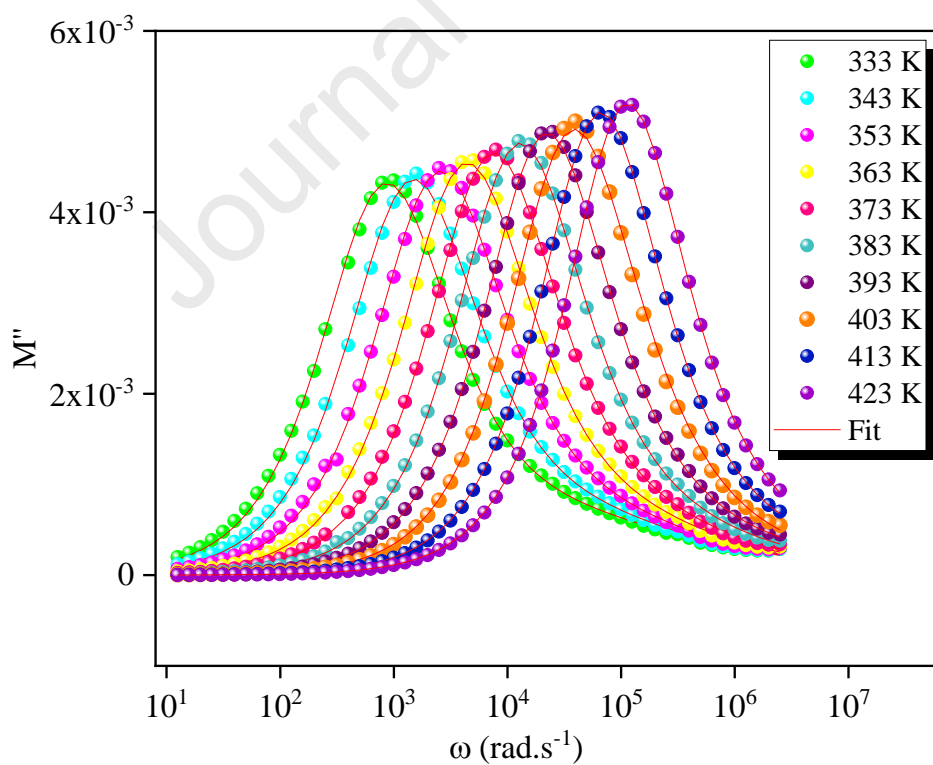


Figure 11 : Frequency dependence of M'' at different temperatures. Solid curves are the best fits to the modulus formalism.

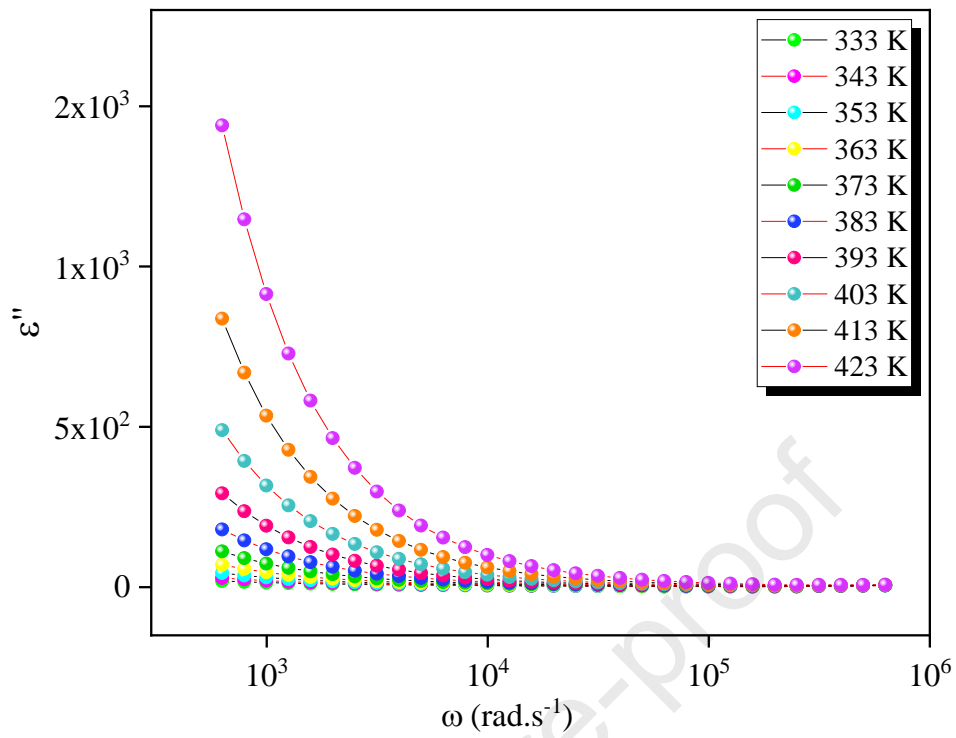


Figure 12: Variation of ϵ'' versus ω at different temperatures.

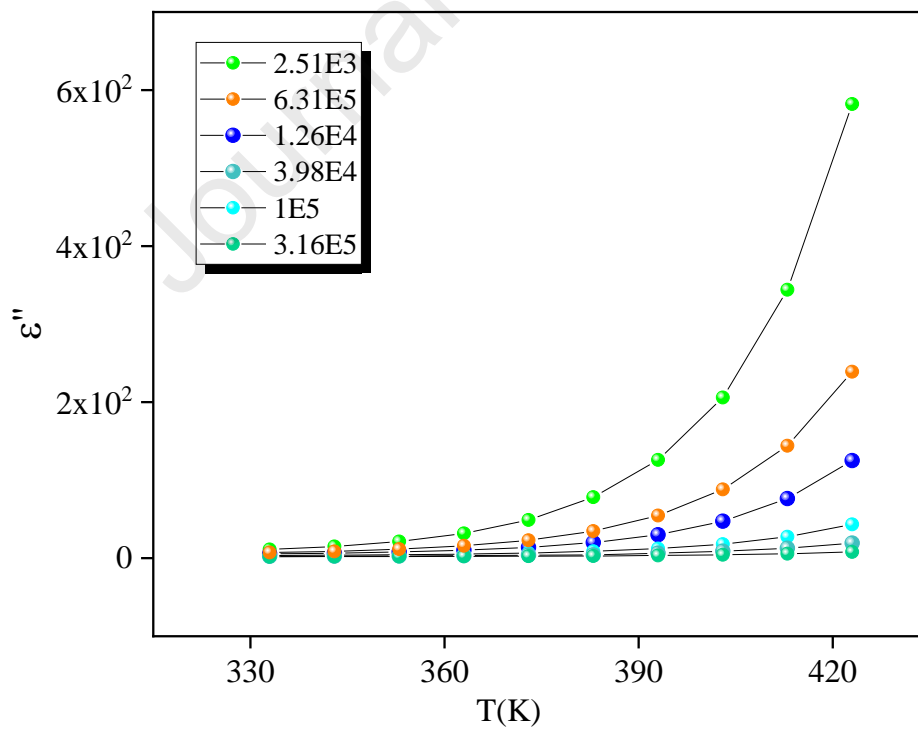


Figure 13: Temperature dependence of the imaginary part of the permittivity at various frequencies.

Highlights

- A new organic-inorganic hybrid compound, $[(C_3H_7)_4P]_2Cd_2Br_6$ has been successfully synthesized by slow evaporation method.
- The thermal analysis reveal one phase transition at $364 \pm (5)$ K.
- The electrical properties are strongly dependent on both temperature and frequency.
- The conduction mechanism is insured by CBH model.

Declaration of Interest Statement

- The authors declare that they have no known competing financial interests or personal relationships that could have appeared to influence the work reported in this paper.

- The authors declare the following financial interests/personal relationships which may be considered as potential competing interests.

Journal Pre-proof